AGU PUBLICATIONS

JGR

Journal of Geophysical Research: Atmospheres

RESEARCH ARTICLE
10.1002/2014JD022658

Key Points:
- Dimming over oceans is quantified with large climate model ensembles
- In the 1990s, anthropogenic dimming affects on average 15.4% of all oceans
- Emissions shape decadal dimming, atmospheric circulations shape seasonal dimming

Correspondence to:
T. N. Dallafior,
tanja.dallafior@env.ethz.ch

Citation:
Dallafior, T. N., D. Folini, R. Knutti, and M. Wild (2015), Dimming over the oceans: Transient anthropogenic aerosol plumes in the twentieth century, *J. Geophys. Res. Atmos.*, *120*, 3465–3484 doi:10.1002/2014JD022658.

Received 2 OCT 2014
Accepted 9 MAR 2015
Accepted article online 18 MAR 2015
Published online 27 APR 2015

Dimming over the oceans: Transient anthropogenic aerosol plumes in the twentieth century

T. N. Dallafior[1,2], D. Folini[1], R. Knutti[1], and M. Wild[1]

[1]Institute for Atmospheric and Climate Science, ETH Zürich, Zürich, Switzerland, [2]Centre for Climate Systems Modeling (C2SM), Zürich, Switzerland

Abstract Anthropogenic aerosols reduce incoming surface solar radiation (SSR), but the magnitude of this effect for reducing sea surface temperatures (SST) is still debated. Using simulations from the global climate model ECHAM5 with the Hamburg Aerosol Module and prescribed SSTs, we quantify anthropogenic aerosol dimming over sea surfaces by comparing ensembles, which only differ in anthropogenic aerosol emissions. We isolate the anthropogenic aerosol effect on SSR with sufficiently large ensemble sizes to provide statistically significant results. The following simulation results are obtained: Dimming plumes extend from their source regions with clear seasonality. The latter is predominantly shaped by atmospheric circulation, while interdecadal changes follow the gradual increase in anthropogenic aerosol emissions. Comparing the 1990s with the 1870s, on average, 9.4% (clear-sky SSR) or 15.4% (all-sky SSR) of the entire ocean surface was affected by anthropogenic aerosol dimming larger than -4 Wm^{-2} (decadal mean). Comparing the same time periods, global average anthropogenic dimming over oceans is -2.3 Wm^{-2} and -3.4 Wm^{-2} for clear-sky and all-sky SSR, respectively. Surface dimming is hemispherically asymmetrical with stronger Northern Hemispheric dimming by 2.3 Wm^{-2} and 4.5 Wm^{-2} for clear-sky and all-sky SSR, respectively. Zonal average clear-sky dimming reaches its maximum (-5.5 Wm^{-2}) near the equator. All-sky dimming peaks at 40°N (-8 Wm^{-2}) and is regionally larger than clear-sky dimming. Regionally, surface dimming can reach values up to 9.5 Wm^{-2} (clear-sky) and 25 Wm^{-2} (all-sky). Results are a contribution toward better quantifying spatially heterogeneous and time-dependent anthropogenic dimming effects on SSTs.

1. Introduction

Between the 1950s and 1980s, downward solar radiation (measured mainly over land) reaching the Earth's surface decreased coincident with increasing anthropogenic aerosol emissions [*Wild*, 2009, 2012], a process also known as global dimming. While greenhouse gases (GHG) are thought to speed up the global hydrological cycle [*Trenberth et al.*, 2007], anthropogenic aerosol dimming may have the opposite effect, namely an attenuation of the hydrological cycle [*Wild and Liepert*, 2010], for instance, through reducing SSTs. The present work is a contribution to the debate on the potential effect of anthropogenic aerosols on SSTs. In order to understand the magnitude of this effect, we here quantify anthropogenic aerosol dimming over oceans over the twentieth century using model experiments with prescribed transient SSTs and transient anthropogenic aerosol emissions. This work is part of a more comprehensive effort to quantify a potential SST signal from global dimming.

Aerosols can reduce the amount of solar radiation reaching the surface through direct aerosol effects, such as absorption, reflection, and scattering, or through indirect effects (see *Lohmann and Feichter* [2005] for a review), such as changes in cloud albedo [*Albrecht*, 1989] and lifetime [*Twomey*, 1977]. Reflection and absorption of solar radiation can cause a cooling of the climate system or, in the case of absorption, a cooling near the surface and a warming aloft [e.g., *Kaufman et al.*, 2002; *Ramanathan and Carmichael*, 2008]. By affecting the vertical temperature profile, the semidirect effect can alter cloud cover and atmospheric stability [e.g., *Hansen et al.*, 1998; *Johnson et al.*, 2004]. Uncertainty still prevails concerning the magnitude of indirect aerosol effects [e.g., *Lohmann et al.*, 2010].

In their review paper, *Yu et al.* [2006] estimate observed direct climate forcing (DCF) of anthropogenic aerosols at the top of atmosphere (TOA) at -1.33 ± 0.82 Wm^{-2}, globally. Over land and oceans, the TOA DCF estimates amount to -1.8 ± 1.5 Wm^{-2} and -1.1 ± 0.5 Wm^{-2}, respectively. The same TOA estimates including all aerosols (natural and anthropogenic) amount to -4.9 ± 0.7 Wm^{-2} and -5.5 ± 0.2 Wm^{-2} over land and

ocean, respectively. Clear-sky DCF due to anthropogenic aerosols at the surface is estimated around −4.2 and $-4.4 \pm 0.6 \mathrm{Wm}^{-2}$ depending on reference used on a global, annual average. *Yu et al.* [2006] define DCF as the perturbation of net (downward minus upward) irradiance over the solar and thermal infrared spectrum by anthropogenic aerosols due to direct aerosol effects. Estimates are based on satellite observations. However, over ocean surfaces and over land in general, *Yu et al.* [2006] complemented satellite retrievals with surface measurements and model simulations due to "lack of measurements of aerosol absorption and difficulty in characterizing land surface reflection."

Compared to long-lived GHG, modeled aerosol lifetimes are much shorter, i.e., between 3.6 and 9 days depending on species [*Koch et al.*, 2009; *Roelofs*, 2012], so that aerosols are not homogeneously mixed throughout the atmosphere. Thus, regional dimming can reach much larger magnitudes than the global average. For instance, over the Arabian Sea, the seasonal average aerosol dimming was measured at $-13 \mathrm{Wm}^{-2}$ [*Ramanathan et al.*, 2001]. Several studies found that, regionally, aerosol effects on the climate system can be larger than GHG effects [*Rotstayn and Lohmann*, 2002; *Ramanathan et al.*, 2005; *Jones et al.*, 2007; *Ramanathan and Feng*, 2009; *Shindell et al.*, 2012].

Multiple studies show evidence that aerosols can drive SST changes [e.g., *Evan et al.*, 2009]. Questions remain on how to reconcile this with other drivers of SST. In global circulation models with interactive oceans, SSTs and radiative forcings show better agreement with observations if anthropogenic aerosols are included [*Delworth et al.*, 2005; *Ramanathan et al.*, 2005; *Cox et al.*, 2008]. Since most anthropogenic aerosols are emitted in the Northern Hemisphere, the arising interhemispheric contrast in dimming was found to increase the interhemispheric SST gradient in modeling frameworks [e.g., *Rotstayn and Lohmann*, 2002; *Jones et al.*, 2007; *Ming and Ramaswamy*, 2011]. Multimodel analyses of the Coupled Model Intercomparison Project phase 3 (CMIP3) model data suggest that the observed interhemispherical Atlantic temperature gradient is unlikely a consequence of internal variability but rather dominated by anthropogenic sulfate aerosols, especially in models including aerosol indirect effects [*Chang et al.*, 2011]. These findings are also confirmed with Coupled Model Intercomparison Project phase 5 (CMIP5) data [*Chiang et al.*, 2013].

Simple thermodynamic models driven by satellite observations have shown that anthropogenic aerosols can induce SST changes in the tropical North Atlantic [*Evan et al.*, 2009]. North Atlantic modeling efforts with a current CMIP5 model (HadGEM2) with a dynamic ocean and explicit aerosol treatment suggest that indirect aerosol effects from anthropogenic and volcanic aerosols accounted for 76% of the multidecadal SST variance, anthropogenic aerosols alone for 66% [*Booth et al.*, 2012]. The authors argue that aerosol-induced SST changes were an important pacemaker of European climate over the twentieth century. This agrees with other coupled ocean-atmosphere-aerosol modeling studies suggesting that anthropogenic aerosol cooling over the North Atlantic counteracted the GHG-induced weakening of the Atlantic Meridional Overturning Circulation in the Ocean [*Cowan and Cai*, 2013]. However, *Zhang et al.* [2013] question findings by *Booth et al.* [2012] because of discrepancies between observed and modeled ocean heat content. Nevertheless, the framework used in *Booth et al.* [2012] was previously shown to reproduce aerosol-induced (direct and indirect effects) surface solar radiation (SSR) dimming trends in accordance with observational data [*Haywood et al.*, 2011]. This is particularly relevant since the aerosol impact on SSTs in each model is affected by the respective representation of aerosol microphysics and indirect effects. This was shown by *Dunstone et al.* [2013] in the context of aerosol effects on North Atlantic Hurricanes. In short, it is still subject to debate whether North Atlantic SSTs are affected by anthropogenic aerosol dimming and, if at all, how large this effect is.

Modeling studies over the Indian Ocean suggest that anthropogenic aerosol dimming cools the northern Indian Ocean, weakening the meridional SST gradient in the Indian Ocean basin. Contrasting with aerosol effects, GHG effects cause a uniform warming throughout the entire Indian Ocean basin [*Ramanathan et al.*, 2005]. The two effects combined result in a weaker meridional SST gradient over the Indian Ocean, which may be responsible for reduced precipitation over the Indian subcontinent [*Chung and Ramanathan*, 2006]. However, *Bollasina et al.* [2011] argue that the aerosol-induced interhemispheric temperature contrast rather than regional SST changes drives the observed regional precipitation changes. Thus, they agree on the generally crucial role of anthropogenic aerosols in masking GHG-induced precipitation increases.

As the example of the Indian Ocean region shows, aerosol-induced SST changes potentially affect precipitation patterns. In the Sahel region, Atlantic SST patterns were found to be important precipitation determinants. CMIP5 models that reproduced North Atlantic SST variability better also predicted Sahel

rainfall better [*Martin et al.*, 2014]. In all models analyzed, Sahel rainfall responses were captured from both natural variability and forced changes. Yet, *Martin et al.* [2014] found that models that included cloud-aerosol interaction and dust-SST-rainfall feedbacks performed better.

In summary, there is a growing body of evidence supporting the hypothesis that aerosol-induced SST changes are possible and pronounced enough to induce changes in atmospheric circulation and precipitation patterns in various regions of the world. However, it is difficult to separate the anthropogenic signal from natural variability. It remains to be understood how to reconcile aerosol-induced SST changes with other drivers of SST in order to understand past SST changes. Here we focus on the question of anthropogenic versus natural aerosol effects on dimming and how they changed throughout the twentieth century. We deliberately postpone the effect of aerosols on SSTs to a following study.

By using a modeling approach to achieve the objective of this work, we benefit from two advantages: First, models provide physically consistent data, which reach further back in time than the available observational data. Second, prescribed SSTs reduce the complexity of the system so that potential feedback mechanisms do not mask out the anthropogenic aerosol dimming. Previous mixed-layer ocean experiments showed that SST responses amplified the climate response to anthropogenic aerosol forcing compared to experiments with prescribed SSTs [*Hsieh et al.*, 2013]. Moreover, by using large ensembles, we are capable of producing statistically robust results.

To find out when, where, and how strongly aerosol dimming over oceans occurs, we apply two approaches to three relevant variables, namely, aerosol optical depth (AOD), clear-sky surface solar radiation (SSR), and all-sky SSR. The first approach involves comparison of ensemble mean values of the entity considered. The second approach relies on comparing probability distribution functions (PDFs) based on quantiles. The aim of this latter approach is to check specifically for locations with particularly strong and persistent anthropogenic dimming. The regions identified thus are likely a subset of the regions quantified with the first approach (via ensemble mean comparisons) and likely underestimate the area affected by anthropogenic aerosols. The second approach is described in more detail in Appendix A. Results are shown in section 3.1 for the ensemble mean and sections 3.2 and 3.3 for the quantile approach. Section 3.4 analyzes the potential role of SSTs for the dimming signals obtained. Results are discussed in section 4.

2. Modeling Framework and Experiments

Atmospheric processes are represented by the general circulation model (GCM) fifth generation ECHAM5 [*Roeckner et al.*, 2003, Version October 2008] from the Max Planck Institute for Meteorology. Temperature, surface pressure, divergence, and vorticity are integrated using spectral discretization with triangular truncation at resolution T42, which corresponds to about 2.8° (~300 km) longitude-latitude resolution. Vertical calculations are performed using finite differences on hybrid-σ coordinates with 19 vertical levels, the uppermost being at 10hPa. Passive tracer transport follows *Lin and Rood* [1996], which is a semi-Lagrangian scheme using Arakawa C-grid staggering and finite differences. Prognostic equations for cloud liquid water, ice, and water vapor are solved after *Lohmann and Roeckner* [1996], and cloud cover is calculated based on *Sundqvist et al.* [1989]. The mass flux scheme follows *Tiedtke* [1989] with modifications by *Nordeng* [1994] issued for convective clouds and convective transport. Shortwave radiation is computed within the *Fouquart and Bonnel* [1980] scheme, and long-wave radiation is computed after *Mlawer et al.* [1997] and *Morcrette et al.* [1998].

Within ECHAM5, the fully interactive Hamburg Aerosol Module, HAM, is implemented [*Stier et al.*, 2005]. HAM represents aerosols through seven lognormal modes containing internally mixed particles of dust (DU), sulfate (SU), particulate organic matter (POM) or organic carbon (OC), sea salt (SS), and black carbon (BC).

Aerosol microphysical processes are computed in the aerosol dynamics and thermodynamics scheme, M7, and comprise nucleation, coagulation, sulfuric acid condensation, and water uptake [*Vignati and Wilson*, 2004]. Removal processes, i.e., dry deposition, sedimentation, and wet deposition depend on particle size, composition, mixing state, and meteorological conditions and are outlined in *Stier et al.* [2005]. Aerosol activation and ice nucleation are computed with the two-moment scheme described in *Lohmann et al.* [2007].

The data analyzed here have previously been analyzed in other contexts, e.g., by *Bichet et al.* [2011] and *Folini and Wild* [2011]. The four ensembles used are summarized in Table 1. Experiments cover the years

Table 1. Setup of the Experiments Used for the Present Analysis[a]

Ensemble Name	Members (#)	SSTs	Anthropogenic Aerosol Emissions	Explosive Volcanoes
ANTH	13	Transient	Transient	Included
CTRL	9	Transient	Constant at 1870	Included
ANTHClim	12	Climatological (1871–1900)	Transient	Included
CTRLClim	3	Climatological (1871–1900)	Constant at 1870	Not included

[a]Except for SSTs and anthropogenic aerosol emissions, the experiments are set up identically. CTRLclim is the only ensemble not to include radiative effects in the stratosphere due to large-scale volcanic eruptions.

1870 to 2000. All experiments have prescribed SSTs so that SST feedbacks cannot affect results. The experiments used for the present analysis are identical except for two boundary conditions: anthropogenic aerosol emissions (either transient or fixed at preindustrial levels) and SSTs. Within each ensemble, the respective members only differ in their starting dates, which lie a few months apart. The atmospheric initialization is always a January climatological mean condition, while external factors such as the Sun's elevation or SSTs correspond to the actual initialization month. The CTRL experiment only includes natural aerosol emissions, while anthropogenic emissions are held constant at year 1870 levels. SSTs are prescribed (either transient or climatological mean values for the years 1871 to 1900). The ANTH experiment also includes anthropogenic aerosol emissions. The suffix "clim" in the ANTHclim and CTRLclim ensembles indicates that climatological instead of transient SSTs are used. Moreover, CTRLclim is the only experiment where no explosive volcano effects are included. Otherwise, the experiments are set up identically to ANTH and CTRL, respectively.

2.1. External Forcings

Radiative effects due to major volcanic eruptions are accounted for by prescribing monthly optical depths in the stratosphere on six latitudinal bands, following *Sato et al.* [1993]. Variations in total solar irradiance are prescribed based on *Solanki and Krivova* [2003]. GHG concentrations are prescribed annually based on observations. Tropospheric ozone concentrations are prescribed monthly as a function of latitude and longitude following *Kiehl et al.* [1999]. Sea surface temperatures and sea ice are prescribed monthly with the *Rayner et al.* [2003] gridded data ($1^\circ \times 1^\circ$ resolution) from the UK MetOffice Hadley Centre for Climatic Prediction and Research.

Historical aerosol emissions of BC, OC, and SO_2 are prescribed using data by the Japanese National Institute for Environmental Studies (NIES) [*Roeckner et al.*, 2006; *Stier et al.*, 2006a; *Nozawa et al.*, 2007; *Folini and Wild*, 2011]. The data set comprises monthly mean aerosol emissions from wildfires, agricultural fires, domestic fuel wood burning, and annual mean emissions from fossil fuel use. Biogenic OC emissions fluctuate within a year but do not change over the years. Dust, sea salt, and dimethyl sulfide (DMS) emissions are derived interactively through the *Tegen et al.* [2002], *Monahan et al.* [1986], and *Nightingale et al.* [2000] schemes, respectively. DMS seawater concentrations stem from *Kettle and Andreae* [2000].

Aerosol lifetimes are comparable with those derived by *Stier et al.* [2005], where lifetimes were 5.4 days for BC and POM, and 3.9 days for SU. In our simulations, aerosol lifetimes estimated as the ratio of the column burden to the total source for 1870 conditions are 5, 5.6, and 4.25 days for OC, BC, and SU, respectively. These lifetimes change over time resulting in 6, 5, and 2.4 days for year 2000 conditions. Aerosol lifetime changes are in line with findings by *Stier et al.* [2006b] for a similar model setup and are explained with nonlinearities in the global aerosol system.

Figure 1 shows the shares of the total global emissions of BC, OC, and SU emitted regionally. The emission regions considered are East Asia, India (including the Arabic subcontinent), North America (East and West Coasts), Africa, and South America (west coast). The regions selected are the source regions of the aerosol plumes, which will be used in the analysis later. We only consider emission regions where aerosols are predominantly advected out to sea. This explains why the sum of all relative contributions in Figure 1 does not equal 1. DU emissions are not shown since land use changes are not included in our setup.

Globally, the African region is the dominant emitter for DU (not shown) and OC but less important for SU emissions. North America was the most dominant SU emitter in the early twentieth century. However, Asia took over this role toward the end of the twentieth century. Africa, East Asia, and India are the dominant BC emitters in descending order.

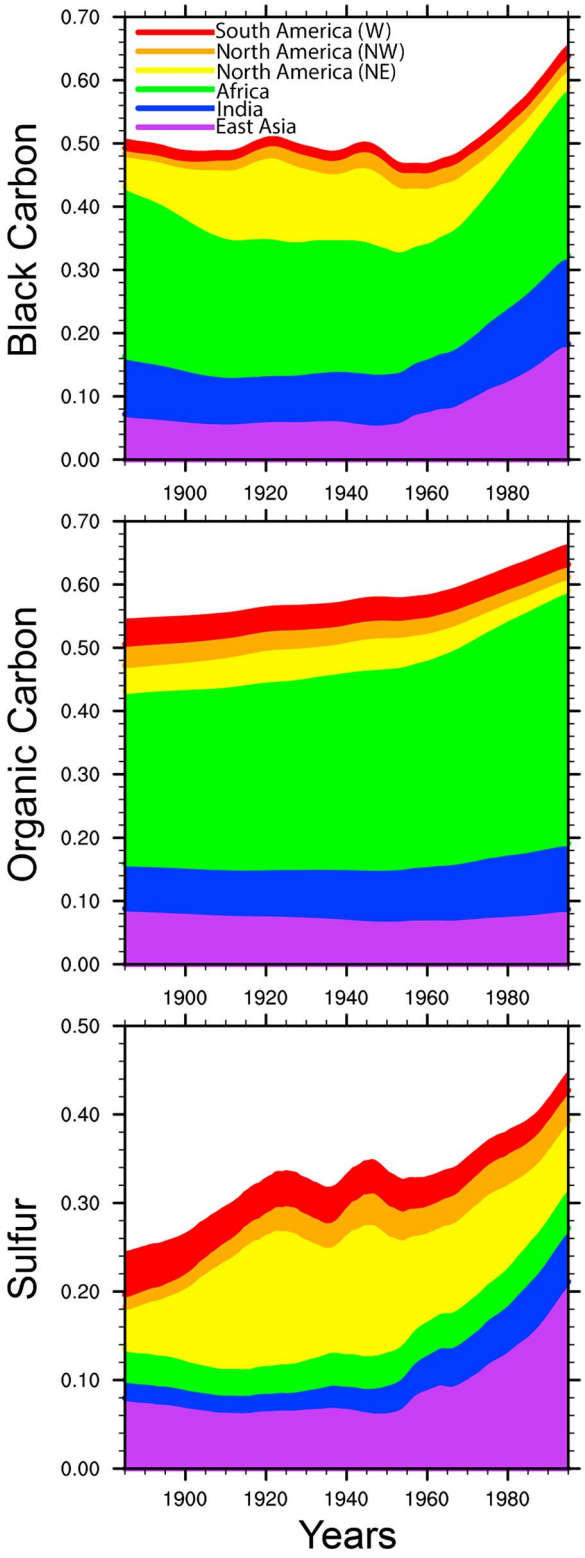

Figure 1. Emissions (mass flux) of black carbon, organic carbon, and sulfur by region relative to the total global emissions of the respective species. Other aerosol components (dust, sea salt, and dimethyl sulfide) do not show a significant anthropogenic trend over time and are therefore not shown. Only regions relevant for anthropogenic aerosol dimming over oceans are considered; hence, the white space in the graph represents the share of emissions from all other regions.

2.2. Comparison With Observational Data

To evaluate our model setup, we compare modeled with remotely sensed clear-sky AOD. For ECHAM5-HAM, AOD has previously been compared with remote sensing retrievals of AOD by *Stier et al.* [2006a], who used a very similar version of ECHAM5-HAM with the same aerosol emission data set (NIES). They find global average AOD (year 2000 mean, land and ocean) of 0.22, slightly higher than observed MISR (Multi-angle Spectroradiometer) and MODIS (Moderate Resolution Imaging Spectroradiometer) data, which yield year 2000 to 2004 means of 0.21 and 0.20, respectively. Our average AOD of 0.21 (year 2000 mean) falls within the range of these estimates. Note in this context that MODIS estimates of AOD are at the higher end of the range of available satellite retrievals [*Myhre et al.*, 2005]. Moreover, the NIES data set contains rather strong aerosol emissions. When using the weaker Aerosol comparison between models and observations (AEROCOM, http://aerocom.met.no/Welcome.html) emission data for year 2000, *Stier et al.* [2005] obtain a lower global average AOD of 0.14 in good agreement with Aerosol robotic network (AERONET) observations. *Stier et al.* [2006a] attribute their higher AODs compared to *Stier et al.* [2005] to differences in the emission inventory and increased dust emissions. In addition, sea salt emissions are about 20% higher in *Stier et al.* [2006a] compared to those in *Stier et al.* [2005] and similar to our sea salt emissions. Note also that in our model setup, global (land and ocean) mean AODs are 0.14 already in year 1870 when anthropogenic aerosol emissions are virtually nil. We can therefore argue that the high AOD is predominantly caused by nonanthropogenic aerosol emissions, which are not the focus of this study.

Figure 2 shows AODs of the model including anthropogenic aerosols (right) compared to observed AODs (MODIS level 3 monthly data, regridded to T42 grids) averaged over 5years

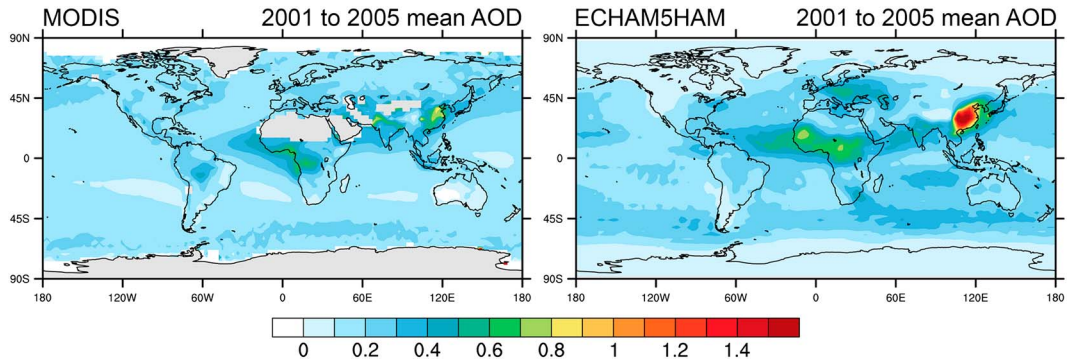

Figure 2. (left) Fiveyear means (years 2001–2005) of AOD at 550nm from MODIS (level 3 data). Grey areas are regions where data were not retrievable, for instance, due to background albedo. (right) Fiveyear means (years 2001–2005) of the modeled AOD of the 13 ANTH ensemble members in ECHAM5-HAM.

(2000 to 2005). Over oceans, a general overestimation of modeled AOD compared to MODIS is apparent, which is particularly distinct off the coast of West Africa and in the southern oceans. Since our focus is on oceans, we briefly look at global ocean average AODs: Modeled optical thicknesses tend to be higher than the remote sensing data by 0.05 on a global average. This positive bias is more pronounced in the Southern Hemisphere (+0.06) than the Northern Hemisphere (+0.03). The high sea salt emissions mentioned above are likely responsible for the Southern Hemispheric bias, which further corroborates our assumption that the high AODs are predominantly caused by natural aerosol emissions rather than overestimated anthropogenic emissions. The strong signal off the African coast is most likely caused by strong BC emissions from forest fires.

The MODIS level 3 data we used for this analysis are derived by sorting the level 2 statistics into $1^\circ \times 1^\circ$ monthly tiles. Collection 5 MODIS AOD observations have an estimated error range of $0.03 \pm 0.05\tau$. However, comparison with AERONET data showed that for an AOD larger than 0.1, the random error is largerthan the above estimate [*Schutgens et al.*, 2013]. This places the above mentioned bias of 0.05 over oceans within MODIS measurement accuracy. Considering that most anthropogenic aerosol dimming happens in the Northern Hemisphere, the model's performance is satisfying for the purpose of this study. We will discuss the relevance of the choice of emission data for our results in section 4.

For the model performance regarding aerosol-cloud interactions, we refer to the detailed study by *Lohmann et al.* [2007]. They show that cloud droplet number concentrations compare reasonably well with observations.

2.3. Quantifying Anthropogenic Aerosol Dimming

Anthropogenic aerosol dimming varies over space and time as a function of aerosol emission and deposition, microphysical and chemical processes, and atmospheric circulation patterns. We quantify anthropogenic aerosol dimming over ocean surfaces using two different approaches, one based on comparison of ensemble means of different experiments and the other based on a threshold criterion to gauge the commonness of anthropogenic aerosol plumes.

For the comparison of ensemble means we conducted a *t* test for significance of dimming and compared ensembles (decadal averages) with and without transient anthropogenic aerosols. Moreover, we quantified the ensemble mean differences in clear-sky and all-sky SSR from different temporal and spatial perspectives (e.g., global, hemispheric, zonal, and decadal).

The analysis focuses on three variables: AOD, clear-sky SSR, and all-sky SSR. Of the three variables, all-sky SSR is physically closest to reality as it also accounts for clouds. Clear-sky SSR is less noisy and easier to analyze but only includes direct aerosol effects. Clear-sky SSR and all-sky SSR are both components of the surface energy balance and thus directly linked to potential SST changes. AOD is a convenient variable for analysis as it does not show the strong latitudinal and seasonal dependence of solar radiation imposed by the Earth's orbit around the Sun. The role of AOD for the diffuse radiation is less straightforward, yet AOD can provide a link between remote sensing observations and computed downward shortwave radiation.

3. Results

3.1. Ensemble Mean Comparison

3.1.1. Global and Hemispheric View

Figure 3 shows 10year running means of globally and hemispherically averaged ocean-only (betweeen 60°N and 60°S) clear-sky and all-sky SSR anomalies for the ANTH and CTRL ensembles listed in Table 1. Anomalies are taken relative to the 10year average of 1870–1879, i.e., the first data point shown. This period is not affected by any major volcanic eruptions. Figures 3a and 3b show the ANTH ensemble where anthropogenic aerosol emissions are transient. Figures 3c and 3d show the CTRL ensemble where anthropogenic aerosol emissions are held constant at 1870s levels. Prescribed SSTs, major volcanic eruptions, and GHG burdens are identical for both ensembles. In all four panels, periods with clearly discernible short-term drops in SSR occur due to explosive volcanoes, such as Krakatau (1883), Agung (1966), El Chicon (1982), or Pinatubo (1991).

If anthropogenic aerosol emissions are present (Figures 3a and 3b), a gradual decrease in clear-sky and all-sky SSR (global ocean mean) is seen, which is especially pronounced after the late 1950s. The total dimming amounts to about -4.1 Wm^{-2} and -3.25 W m^{-2} for clear-sky and all-sky SSR, respectively. Dimming estimates are derived by subtracting the 1870s ocean-only 10year mean (first data point of the respective time series in Figures 3a and 3b) from the 1990s ocean-only 10year mean (last data point of the time series) of the same ensemble. If no anthropogenic aerosols are included, the corresponding clear-sky dimming amounts to -1.8 W m^{-2} (Figure 3c), while no dimming is seen for all-sky SSR (Figure 3d). The dimming seen in Figures 3c and 3d is a consequence predominantly of major volcanic eruptions as well as other factors such as water vapor content.

Figures 3e and 3f show the difference between the absolute values of the 10year running mean time series, ANTH minus CTRL. Since the two ensembles only differ in their anthropogenic emissions, the dimming seen in those panels is solely anthropogenic. Most notably, the effect of explosive volcanoes (and other factors) is removed from the time series. The clear-sky SSR dimming signal due to anthropogenic aerosols is -2.3 Wm^{-2} and therefore -1.8 W m^{-2} weaker than the above total dimming estimate of -4.1 Wm^{-2}. The all-sky dimming signal remains nearly unchanged at -3.4 Wm^{-2} compared to the above estimate.

Modeled global mean (land and ocean) total dimming estimates including natural aerosols from other studies are between -1 W m^{-2} and -4 W m^{-2} [*Romanou et al.*, 2007]. Considering that we are looking at ocean-only dimming, this places our all-sky estimates of -3.25 W m^{-2} at the higher end of the range. However, the dimming estimates in *Romanou et al.* [2007] cover a slightly shorter time span (twentieth century only), while our estimates are taken relative to the 1870s. Note also that global averages of aerosol-induced dimming of SSR should be interpreted with caution because global means mask strong spatial and temporal variability.

Surface dimming (bottom of atmosphere) is generally larger than the TOA signal, especially when absorbing aerosols are present. TOA net all-sky shortwave radiation decreases by -0.9 W m^{-2} (-1.3 W m^{-2} for clear-sky TOA net shortwave radiation) in the ANTH ensemble between the 1870s and the 1990s. Strictly speaking, this estimate is not a radiative forcing as defined by *Ramaswamy et al.* [2001] and used in *Intergovernmental Panel on Climate Change* (*IPCC*) [2013], i.e., "the change in net (down minus up) irradiance (solar plus longwave; in W m^{-2}) at the tropopause after allowing for stratospheric temperatures to readjust to radiative equilibrium, but with surface and tropospheric temperatures and state held fixed at the unperturbed values." Our estimates only cover the shortwave spectrum. Moreover, we allow the troposphere to adjust. Our estimate is thus not directly comparable to the corresponding estimates in *IPCC* [2013]. We nevertheless add the TOA anthropogenic aerosol radiative forcing estimates to put our results in perspective: According to the latest IPCC assessment report, TOA anthropogenic aerosol radiative forcing has its median at -0.27 W m^{-2} [-0.77 to -0.23] for aerosols and precursors. Cloud adjustment due to aerosols is estimated to cause another -0.55 W m^{-2} [-1.33 to -0.05] radiative forcing [*IPCC*, 2013].

After the 1950s, SSR decreases more strongly in the Northern Hemisphere than in the Southern Hemisphere (Figures 3a, 3b, 3e, and 3f). This is temporally coincident with emerging anthropogenic aerosol emissions and not seen in Figures 3b and 3c, where no anthropogenic emissions are included. Clear-sky SSR dimming (Figure 3a) in the Northern Hemisphere is -5.4 W m^{-2} compared to -3.1 W m^{-2} in the Southern Hemisphere, which translates into a 2.3Wm^{-2} difference in surface dimming between the two hemispheres. This hemispherically asymmetric dimming is even more pronounced for all-sky SSR (Figure 3b): The Northern

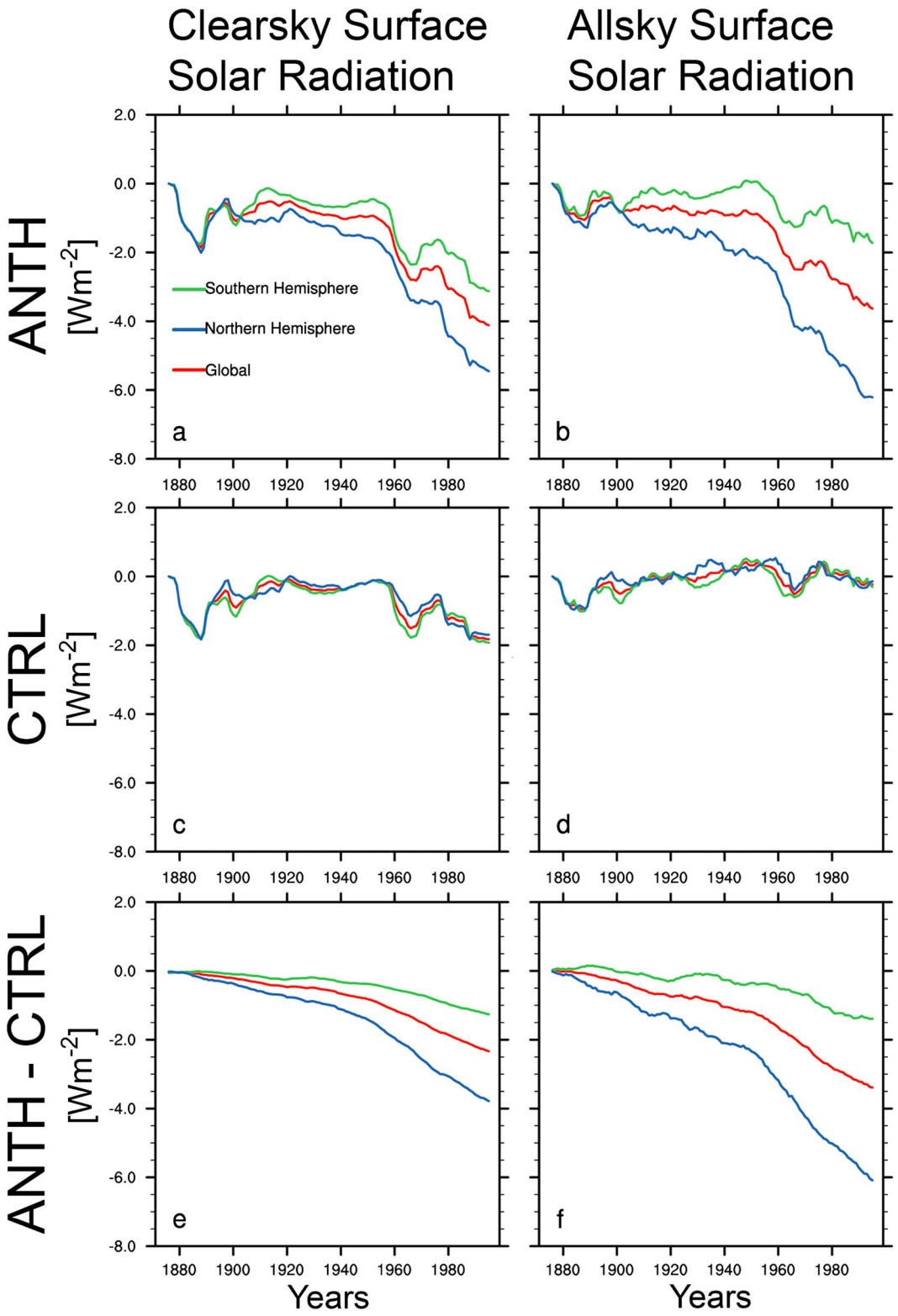

Figure 3. Time series of 10year running means for (a, c, and e) ocean-only clear-sky SSR and (b, d, and f) ocean-only all-sky SSR: Global (red), Northern Hemisphere (blue), and Southern Hemisphere (green) anomalies with respect to the first data point of the respective global ensemble mean time series (i.e., 1870s average). Figures 3c and 3d stem from ensembles with anthropogenic aerosol emissions held constant at 1870 levels, while Figures 3a and 3b had transient anthropogenic aerosols included. Figures 3e and 3f show the differences between the two data sets (ANTH minus CTRL) for clear-sky and all-sky SSR.

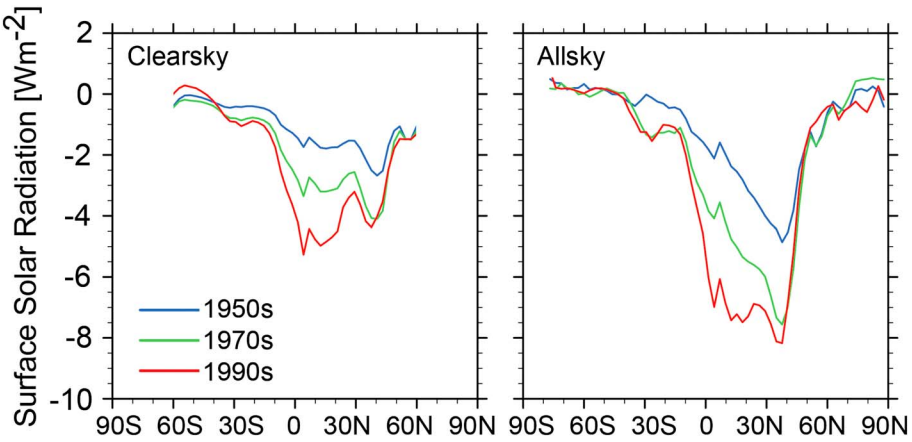

Figure 4. Zonally averaged surface dimming for ocean-only clear-sky and all-sky SSR. Each line in the plots represents the ensemble mean absolute difference in (left) clear-sky SSR and (right) all-sky SSR between CTRL and ANTH averaged over a decade. CTRL values were subtracted from ANTH values. The ensembles compared have identical transient SSTs, explosive volcanoes, and greenhouse gas concentrations but do differ in anthropogenic aerosol emissions. Clear-sky SSR data beyond 60° latitude were omitted due to sea ice cover changes (for more details, see section 3.1.2).

Hemisphere dimming is −6.2 W m^{-2}, and Southern Hemisphere dimming is −1.7 W m^{-2}, resulting in an overall increase in dimming asymmetry of 4.5Wm^{-2}.

The single ensemble members behave similarly when considering ocean-only 10year averages with the most extreme members only differing by an average over the entire study period of 0.7 W m^{-2} and 0.27 W m^{-2} for clear-sky and all-sky SSR, respectively. These values do not change substantially over time and are similar for both ANTH and CTRL. The respective standard deviations are rather small for both ensembles with 0.3 W m^{-2} and 0.08 W m^{-2} for clear-sky and all-sky SSR, respectively (average standard deviation over the entire study period). The wider spread seen for clear-sky SSR can be explained with the stronger impact of volcanic eruptions on this variable.

3.1.2. Zonal View

Figure 4 shows the difference between the ANTH and CRTL ensemble means, zonally averaged over oceans (note that the southern oceans cover a larger area than the northern oceans). Each line represents a decadal average. For better readability of the graph, only selected decades are shown. Clear-sky SSR dimming values beyond 60° latitude have been removed. Clear-sky SSR in our modeling framework needs to be derived during postprocessing from net clear-sky surface shortwave radiation and surface albedo. It is thus affected by albedo changes at the edges of prescribed sea ice.

The spatially inhomogeneous nature of anthropogenic aerosol dimming is already evident from the zonal perspective. In lower latitudes, all-sky SSR dimming is more pronounced than clear-sky SSR dimming. The strongest clear-sky SSR dimming (−5.5 Wm^{-2}) is seen in the 1990s near the equator, which is predominantly due to aerosol outflow from West Africa, and the Indian and Arabian subcontinents. For all-sky SSR, the most distinct peak (−8 Wm^{-2}) develops at 40°N, which is dominated by dimming off the coast of East Asia and, to a lesser extent, North America. Zonal mean dimming in this study can be up to twice as strong as the global average.

The strongest dimming increase with time is seen in the northern extratropics between the 1950s and 1970s, while the strongest increase in the tropics is seen between the 1950s and 1990s (not shown). Brightening, as was observed over most major regions in the Northern Hemisphere between 1980 and 2000 [*Wild*, 2012], is seen in the northern hemispheric midlatitudes (40°N–60°N, see Figure 4). Comparing all ocean-only monthly data of the ANTH ensemble between 40°N and 50°N between the years 1960 and 1979 with the same data covering the years 1980–1999 yields a significant difference (derived with a two-sample Kolmogorov-Smirnov test) between the two data sets. Thus, the brightening in the northern midlatitudes is significant.

3.1.3. Geographical Pattern

The spatial and temporal heterogeneity of anthropogenic aerosol dimming over oceans is illustrated in Figure 5. It displays difference maps for AOD (Figures 5a–5d), clear-sky SSR (Figures 5e–5h), and all-sky SSR

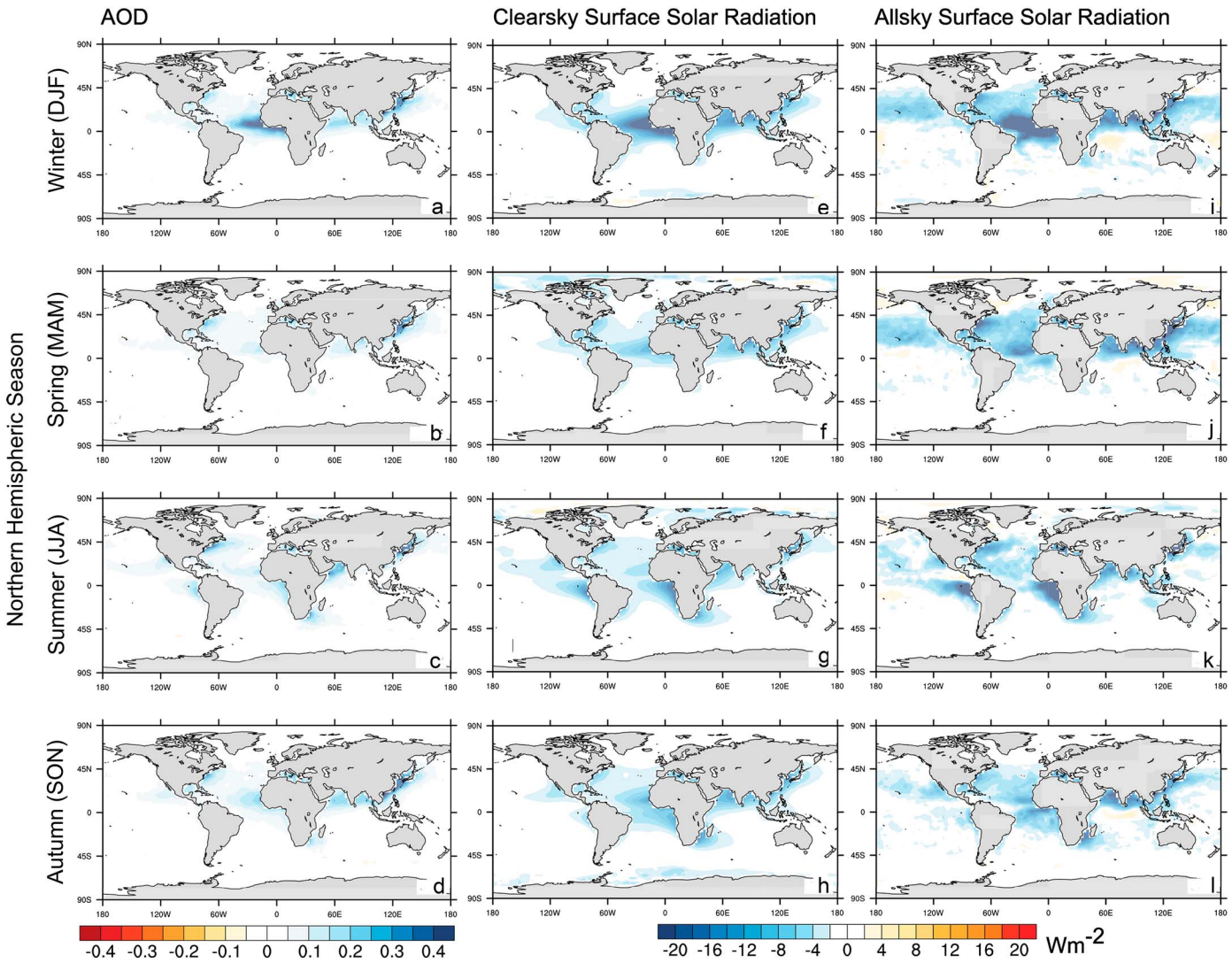

Figure 5. (a–d) Increase in AOD for the 1990s between CTRL and ANTH, seasonally averaged over the entire 1990s. (e–h) Difference between the two clear-sky SSR ensemble means (ANTH − CTRL), seasonally averaged over the entire 1990s. (i–l) Same as Figures 5e–5h but for all-sky SSR. Prescribed SSTs, explosive volcanoes, and greenhouse gas concentrations were identical and transient in both CTRL and ANTH.

(Figures 5i–5l), respectively. The maps show seasonal averages over the 1990s of the ANTH ensemble mean minus the CTRL ensemble mean. Each row of panels in the plot is representative of a season as indicated on the left-hand side of the panel. Since ensembles ANTH and CTRL only differ in anthropogenic aerosol emissions, the signal can be interpreted as solely anthropogenic. Potential changes in SSR due to SSTs or explosive volcanic eruptions are removed. Blue hues in Figure 5 represent dimming or increased AOD, whereas yellow hues represent brightening or decreased AOD. Note that most SSR areas with a dimming larger than -4 W m^{-2} tested significant (*t* test between ensemble members at 95% confidence interval) in Figure 5. Brightening (yellow hues) with respect to 1870s levels is only seen for all-sky SSR in a few locations, for instance, over the equatorial Indian Ocean (Figures 5i and 5l). However, unlike the dimming signals, the brightening signals are barely significant and are not seen in each one of the ensemble members of ANTH (1990s average, compared to 1990s CTRL ensemble mean).

Three characteristics stand out. First, aerosol dimming shows plume-like structures extending over the oceans reaching maximum values of more than -20 Wm^{-2} for clear-sky SSR (i.e., 5 times the global mean value). The plumes are attached to major emission regions on the continents, for instance, biomass burning in Africa or fossil fuel emissions on the Indian subcontinent. Second, aerosol dimming shows a clear seasonal signal. However, seasonality is not equally distinct for each of the plumes. For instance, the plume off

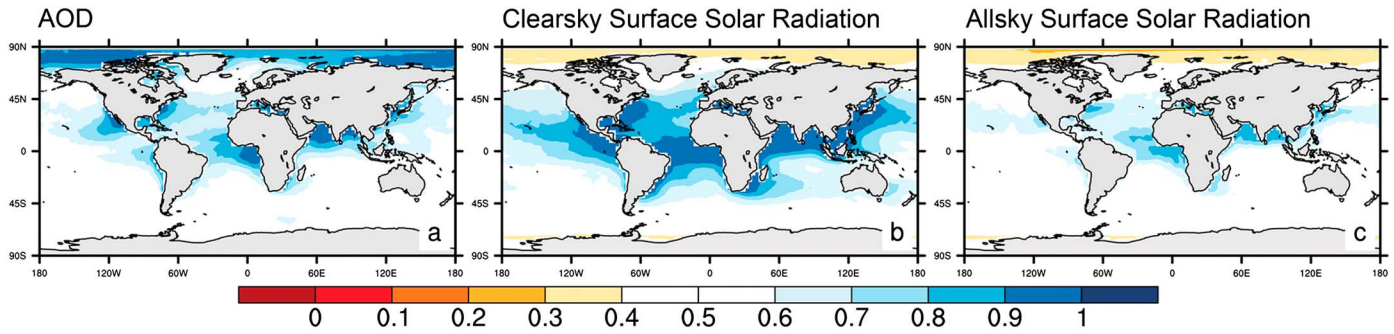

Figure 6. (a) Fraction of months in the 1990s where AOD in the ANTH ensemble data set was larger than the 50th quantile of the respective CTRL AOD over the entire time span (1870 to 2000). (b and c) Analogous to Figure 6a, fraction of 1990s ANTH data that was below the 50th quantile in CTRL for clear-sky SSR (Figure 6b) and all-sky SSR (Figure 6c).

West Africa shows a much stronger seasonal variability than the plumes off the coast of East Asia or North America. This raises the question of temporal persistence of the respective plumes. Third, the all-sky SSR anthropogenic dimming signal is clearly evident but generally more noisy. It is also seen in remote marine regions (see Figures 5i–5l), in particular over the North Pacific or the North Atlantic, where dimming signals of up to -4 W m^{-2} are evident. All-sky SSR includes clouds, so that cloud cover changes and changes in cloud optical properties can have an effect. We will use the region of origin for later naming of the respective plume areas in sections 3.2 and 3.3 where we will scrutinize this further.

3.1.4. Ocean Area Affected

We define an average SSR reduction of -4 W m^{-2} as an identification criterion for anthropogenic dimming. This value was chosen based on the result of the *t* test conducted above, where a dimming of -4 W m^{-2} is generally significant at the 5% significance level. The area of all anthropogenic dimming plumes summed up during the 1990s accounts for 9.4% and 15.4% of the entire ocean surface for clear-sky and all-sky SSR, respectively. Over the North Atlantic (entire width between 30° and 60°N), the area affected by clear-sky and all-sky dimming accounts for 8.9% and 38% of the entire area, respectively.

3.2. Frequency-Based Plume Regions: The Basic Idea

The analysis presented above demonstrates that dimming over oceans with our model setup exists, comes in plumes, shows seasonality, increases over time, and tends to be regionally stronger under all-sky than clear-sky conditions. However, it does not show how common the dimming is. The mean values considered in the analyses above may be distorted by a few very extreme exceptions rather than reflecting what regularly happens since it does not strongly account for the role of spread and extremes with respect to the mean. We therefore use a different approach, which is based on the quantiles of the respective data distributions (for details on the approach see section 2.3 and Appendix A).

Figure 6 illustrates what fraction of monthly time steps of the ANTH data set (1990s data) is above (for AOD) or below (for SSR) the 50th quantile of the respective CTRL data set (entire simulation period). The regions identified with this approach are similar to the ones seen in Figure 5, which shows ensemble mean differences. Compared to Figure 5, Figure 6 contains additional information about the overlap of the two distributions compared: If a fraction of 1 is reached (darker blue shades), all of the ANTH data lie above the 50th quantile of the CTRL data. Such values are reached in regions where we expect strong anthropogenic aerosol dimming. In remote regions, about half of the data exceed the 50th quantile, which makes sense since we do not expect the two data sets to differ strongly in those areas. Note how the plume areas for AOD (Figure 6a) and clear-sky SSR (Figure 6b) show much darker shades than those for all-sky SSR (Figure 6c). The AOD signal is more pronounced when the share of median exceedances is counted rather than comparing means (Figures 6 and 7). However, the shape of the AOD distribution is not symmetrical as it is bounded at zero. All-sky SSR monthly data have a wider spread than clear-sky SSR leading to the two data sets (CTRL and ANTH) having more overlap. Consequently, the 50th quantile is less often exceeded. Therefore, all-sky SSR dimming shows a more extended signal when ensemble mean values are considered instead of exceedance fractions.

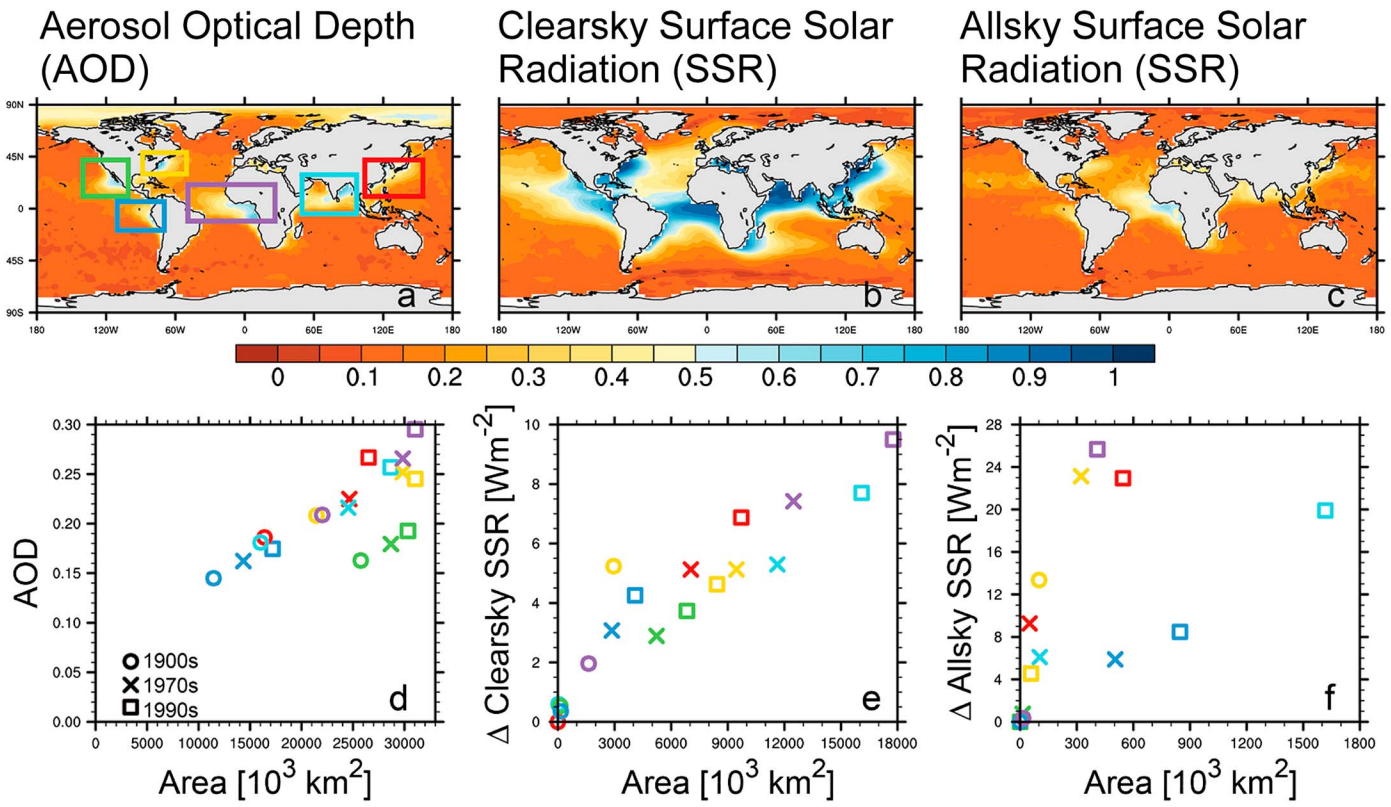

Figure 7. (a–c) As in Figure 6but with respect to the 90th quantile of the reference distribution. (d–f) Evolution of anthropogenically influenced plume size (horizontal extent) and intensity over time (decadal averages) for AOD, clear-sky, and all-sky SSR. Round markers represent the 1900s, crosses the 1970s, and squares the 1990s. Color coding of the markers is the same as in Figure 7a.

3.3. Anthropogenic Aerosol Plume Regions in the Twentieth Century

In order to identify intense and commonly occurring anthropogenic aerosol plumes, we extended the analysis from section 3.2. We shift the threshold quantile from the 50th to the 90th quantile of the CTRL distribution based on the assumption that anthropogenic aerosol dimming manifests itself in the extremes of the respective distribution. Furthermore, we define that half of the ANTH data (50% exceedance fraction) at the respective grid point need to exceed the 90th quantile of CTRL for a grid box to qualify as anthropogenically influenced. This would translate into an average anthropogenic aerosol plume occurrence every second year for that specific month. The result of this analysis is shown in Figures 7a–7c. The maps show what share of 1990s ANTH data exceeded the 90th quantile of the 1870s to 1990s CTRL data set. Blue values indicate regions with an exceedance fraction higher than 50%.

We select six plume regions, which are named after the emission region they originate from. The respective plume regions are indicated in Figure 7a: the Northeast American Plume (yellow), the Northwest American Plume (green), the West African Plume (purple), the East Asian Plume (red), the Indoarabic Plume (cyan), and the Southwest American Plume (blue). Over the Atlantic, it is at times difficult to draw a clear boundary between the aerosol plume originating from West Africa and the one off Northeast America. We choose 30°N as a boundary between the two plumes, which is roughly coincident with the northernmost extent of the Hadley cell.

Whether SST changes can be induced depends on the area over which SSR dimming is applied, its time span, and its intensity. Of course, the circulation patterns of the ocean and other factors such as long-wave radiation also play an important role. However, this is beyond the scope of this work. How the horizontal extent and intensity of the respecitve plumes evolved over time is summarized in Figures 7d–7f. For better readability of the graphs, only three selected decades are shown. Intensity is defined as the average total AOD or the average SSR dimming over the entire plume area. Note the differences in scale between the different variables. Each data point represents the respective size and intensity of each plume (color coded) for different decades (1900s, circle; 1970s, cross; and 1990s, square). Of course, larger and more intense

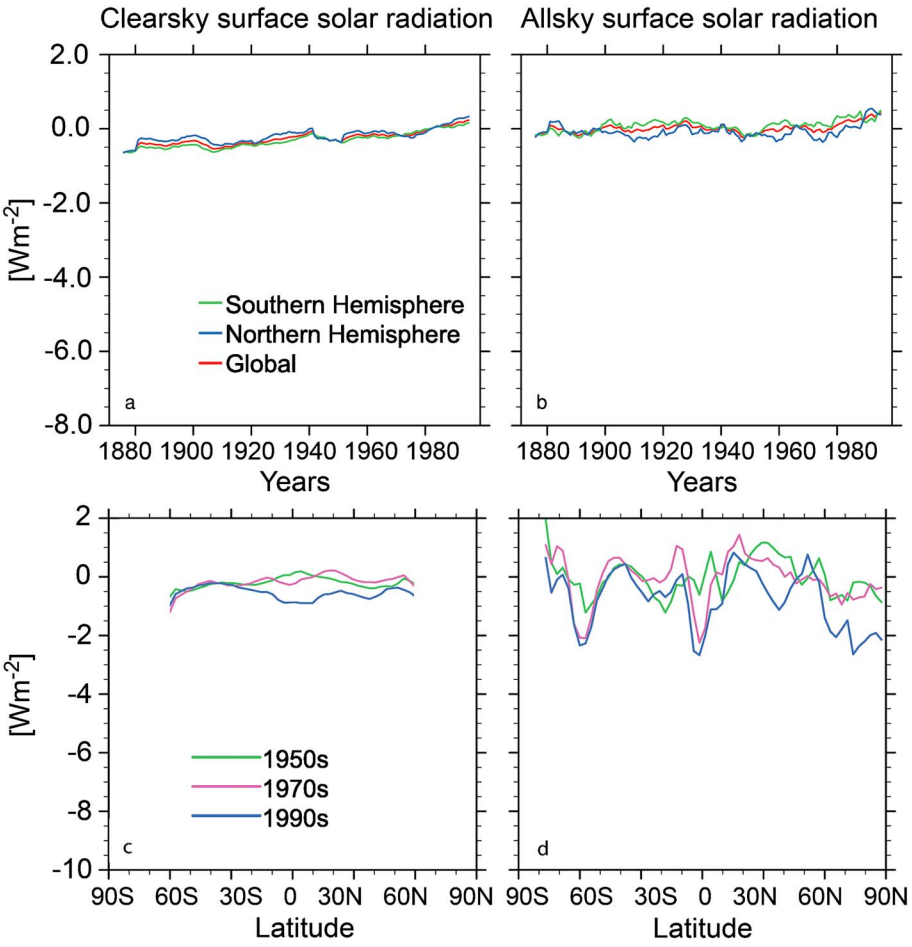

Figure 8. (a and b) Anologous to Figures 3e and 3f), 10 year ocean-only running average time series of differences in clear-sky (Figure 8a) and all-sky (Figure 8b) SSR between the ANTH and ANTHclim ensemble. (c and d) Analogous to Figure 4, zonally averaged surface dimming for ocean-only clear-sky and all-sky SSR. Each line represents a selected decadal average difference between the ANTH and ANTHclim ensemble means for clear-sky SSR (Figure 8c) and all-sky SSR (Figure 8d). The two ensembles compared only differ in their SSTs (transient versus climatological).

plumes can have a larger impact on SSTs so that plumes near the top right corner of the panels are potentially more relevant in terms of SST effects. For AOD (Figure 7d) and clear-sky SSR (Figure 7e), the plumes follow a nearly linear trajectory over time with both size and intensity increasing over the decades. For these two variables, the Northeast American Plume (yellow) was among the largest and most intense regions at the beginning of the twentieth century (circles), while it was surpassed by other regions by the end of the last century and even showed a slight reduction in intensity from the 1970s (crosses) to 1990s (squares). Thus, when comparing the different plumes, a shift in dominant dimming regions happened over the twentieth century from Northeast America to West Africa (purple), Indoarabia (cyan), and East Asia (red).

While AOD and clear-sky SSR behave similarly, all-sky SSR (Figure 7f) does not show such linear trajectories. Nevertheless, the most pronounced plume regions for the 1990s (squares) remain the same as for the other two variables. Moreover, the brightening between the (1970s and 1990s) for the Northeast American Plume (yellow) is much more distinct than that seen for AOD (Figure 7d) or clear-sky SSR (Figure 7e). Note also that the all-sky plumes show a much smaller spatial extent than clear-sky SSR or AOD plumes but have a much stronger dimming signal than clear-sky SSR plumes. This behavior can again be explained by the nature of the all-sky SSR data set, which has a wider spread than the clear-sky SSR data set so that the anthropogenic signal is more difficult to isolate (see section 3.2).

3.4. Sensitivity of Dimming Toward SST Changes

In the analysis results above, SSTs as potential drivers of SSR dimming were largely omitted as we compared ensembles with identical prescribed SSTs. However, it is possible that aerosol-induced SST changes

or aerosol-induced changes in prevailing ocean currents may feed back onto the dimming signal, for instance, due to circulation changes. Therefore, we here compare two ensembles, which only differ in their prescribed SSTs.

Figure 8 shows the differences between the two ensembles ANTH minus ANTHclim. The latter ensemble has climatological SSTs (1871 to 1900 mean), while the former has transient SSTs prescribed. Otherwise, the two ensembles are set up identically (see Table 1).

The time series in Figures 8a and 8b were derived the same way as in Figure 3 (section 3.1.1). The zonal averages shown in Figures 8c and 8d are analogous to the ones in Figure 4. As can be seen in all four panels, no clear trend is evident for clear-sky and all-sky SSR both globally and zonally (ocean-only average). A slightly positive trend is seen for clear-sky and all-sky SSR (Figures 8a and 8b), which may be due to SST-induced circulation changes. Potential changes in water vapor content can be ruled out as a cause since ANTH has a slightly higher water vapor content compared to ANTHclim. Therefore, one would expect a reduction in SSR when subtracting ANTHclim from ANTH since absorption of incoming solar radiation through water vapor would cause dimming.

For clear-sky SSR, zonal average differences due to SSTs are within $\pm$ 1 W m^{-2} (Figure 8c). As explained in section 3.1.2, clear-sky SSR dimming at latitudes higher than 60° is omitted. For all-sky SSR (Figure 8d) the sensitivity is similar, except for the lower latitudes and latitudes higher than 60° where differences up to $\pm$ 2 W m^{-2} are seen.

When comparing Figures 3 and 4 with Figure 8, especially after the 1950s, the anthropogenically induced aerosol dimming outweighs any potential SST-induced effects on dimming so that anthropogenic aerosol dimming is still detectable. This is also in line with *Hsieh et al.* [2013], who found anthropogenic aerosols to have a far stronger effect on dimming than SST changes. The geographical patterns of dimming remain roughly the same regardless of SST choice (not shown).

4. Discussion

In this work, we analyzed the characteristics of anthropogenically induced aerosol dimming over sea surfaces within our modeling framework, ECHAM5-HAM.

Two strengths of our approach are the ensemble size and the long time spans covered. This allows for statistically significant quantification of anthropogenic aerosol dimming on a decadal basis over the twentieth century. With our experimental setup, the anthropogenic aerosol signal in SSR and AOD was detectable, not least because we could rule out other sources of variability such as explosive volcanic eruptions or SST changes.

Results yielded an average anthropogenic aerosol dimming with respect to year 1870 of -2.3 Wm^{-2} and -3.4 Wm^{-2} (oceans only) for clear-sky and all-sky SSR, respectively. An additional clear-sky SSR dimming of -1.8 W m^{-2} may be attributed to other factors such as explosive volcanic eruptions or SST changes. Note that the time series shown in Figure 3 are 10 year running means of ocean-only mean values. The rate of change in anthropogenically induced dimming is smaller in magnitude but more permanent than that due to volcanic eruptions (short-term drops in SSR). This is explained with the more sustained nature of anthropogenic aerosol emissions. This behavior reflects the characteristics of the respective emission sources. The global average (ocean-only) surface dimming in our simulation is at the higher end of the range of global dimming (-1 W m^{-2} to -4 W m^{-2}) seen in other modeling frameworks, which also took into account land points [*Romanou et al.*, 2007]. However, it is in line with observational and literature data shown in *Wild* [2012] and section 1. Moreover, modeled AODs are within the uncertainty range of remote sensing observations (MODIS) over oceans, so that the model's performance can be viewed reasonable.

Comparing ensemble means of the ANTH and CTRL experiments showed that ensembles differed significantly on a regional scale (derived via *t* test) for both variables, clear-sky and all-sky SSR. However, the ensemble mean perspective does not show how common dimming is as it omits the spread of data. Therefore, we look at probability density functions of monthly SSR and AOD on the grid box level. Assuming that anthropogenic aerosol dimming manifests in the tails of the respective distributions, we define a strict criterion for anthropogenic aerosol dimming to identify only regions where a strong anthropogenic aerosol signal is experienced for a large fraction of time. These two characteristics are relevant if we assume that only a sufficiently large and persistent dimming can lead to an SST change.

The all-sky SSR signal is more distinct when comparing ensemble means (Figure 5) than when applying the quantile approach (Figure 7). This is explained with changes in cloud cover and cloud optical properties, which have a larger impact on SSR than direct aerosol-induced surface dimming. Moreover, not all of the changes in all-sky SSR can be attributed to direct, indirect, and semidirect aerosol effects. Other factors such as circulation changes may have an impact on clouds as well. Hence, the impact of anthropogenic aerosols on all-sky SSR does not necessarily manifest in the tails of the distribution, which our quantile approach focuses on.

Aerosol emission strength, aerosol composition, size, lifetime, and the prevailing atmospheric circulation influence timing, location, and strength of anthropogenic aerosol dimming in our model. The globally averaged ocean-only dimming signal seen in Figure 3 is dominated by emissions from Africa, East Asia, and India. They have become more dominant over the twentieth century, while North America, which was dominant in the beginning of the century, has become less important. This is also reflected in the temporal development of the respective plume regions in Figure 7. Due to atmospheric circulation patterns, anthropogenic aerosol emissions are not persistently advected out to sea so that on a month-to-month basis, anthropogenic aerosol dimming over certain ocean regions does not persist throughout the entire year. This effect can be amplified through cloud-aerosol interactions, which may be significant, especially in remote regions [e.g., *Wild*, 2012].

The emission inventory is a crucial component in the model setup. The NIES inventory used here is on the stronger side, especially in terms of biomass burning emissions, for instance, off West Africa. In our modeling framework BC emissions from forest fires are the dominant aerosol emission component leading to the dimming signal (not shown). In ensembles where these emissions are absent, the plume off West Africa is strongly reduced. Moreover, aerosol aging (e.g., BC can be coated with sulfate and thus become soluble) is included in HAM and may also have an effect. Nevertheless, we find in our data that the NIES data set is not constantly too strong. For instance, when comparing our modeled monthly AODs off the West African coast with monthly mean MODIS observations, the expected overestimation is only seen during the boreal summer months over the northern tropical Atlantic, while austral summer month AODs over the southern tropical Atlantic are underestimated. Note that West African emissions account for a considerable share of all global emissions.

In ECHAM, it was shown that aerosol emission composition affects aerosol lifetime and that this effect is nonlinear and shaped by aerosol microphysical processes [*Stier et al.*, 2006b]. Moreover, it was recently shown that for clear-sky SSR in simulations with the Geophysical Fluid Dynamics Laboratory (GFDL) model, differences in aerosol treatment, especially aging and mixing, can have an equally strong effect as differences in aerosol emissions [*Persad et al.*, 2014]. However, it was shown that applying the same emission inventory (AeroCom) to different models does not reduce the spread of the model results [*Textor et al.*, 2007]. Thus, model-inherent processes can play a more dominant role at determining aerosol characteristics and resulting forcings. This agrees with findings by *Stier et al.* [2013], who could show that "host model uncertainties" (i.e., surface albedo, clouds, radiative transfer) account for about 36% of the forcing diversity in their experimental setup pointing out that not all model diversity stems from aerosol representation. Thus, even though the choice of aerosol emission inventory has a large impact on results, there is a host of other model characteristics that do so as well.

The seasonal signal in anthropogenic aerosol dimming shows a strong imprint of atmospheric circulation (e.g., Figure 5). The West African plume is predominantly shaped by the migration of the Intertropical Convergence Zone in the course of a year. Additionally, the seasonality of wildfire emissions crucially influences the plume's behavior. Basically, all low-latitude plumes exert such a behavior. For these regions, anthropogenic aerosol dimming can cease for certain months completely. The plumes further north (Northeast American and East Asian Plumes) are more persistent throughout the year.

Put simply, aside from aerosol composition effects, which are not discussed here, anthropogenic aerosol dimming is dominated by emission strength on an interdecadal scale and by atmospheric circulation patterns on a seasonal scale. We stress again that the results presented were obtained with only one model, ECHAM5-HAM. Model-inherent factors influence the dimming signal encountered. Thus, results presented here should be viewed as a contribution to the ongoing discussion about anthropogenic aerosol effects on SSTs.

5. Conclusions

In the presented work we characterized anthropogenic aerosol dimming at the sea surface over the twentieth century since early industrialization (1870s) using a general circulation model with explicit aerosol representation (EHCAM5-HAM). We compared ensemble experiments with prescribed SSTs, which only differ in their anthropogenic aerosol emissions. Our experimental setup allowed us to isolate the anthropogenic aerosol signal over 130 years and derive statistically significant results thanks to sufficiently large ensemble sizes. We characterized anthropogenic aerosol dimming from a global, hemispherical, zonal, and regional perspective over the decades and seasonally, yielding information about the commonness, location, persistence, and intensity of the aerosol-induced dimming over oceans within the limitations of the modeling framework.

Our results are a contribution to the debate on whether anthropogenic aerosols are capable of affecting SST patterns through a reduction of incoming solar radiation at the sea surface. Evidence for such influences so far is rather inconclusive not least because the anthropogenic aerosol signal is difficult to detect. According to our data, at present day, 9.4% or 15.4% of all ocean surfaces experience anthropogenically induced surface dimming beyond -4 W m^{-2} for clear-sky and all-sky SSR, respectively (ocean-only 10year means). This is a substantial share of the ocean surface and therefore deserves a closer look.

The presented results are a first step in identifying anthropogenic aerosol dimming effects on SSTs. We quantified the heterogeneity of the anthropogenic aerosol dimming over sea surfaces, and we described how the anthropogenic contribution to SSR changes in those areas evolved over time. In particular, we found that the signal is also significant in rather remote regions for all-sky SSR. The heterogeneity of the aerosol-induced dimming potentially affects precipitation and circulation more effectively than the homogeneous warming caused by GHG. We stress, however, that despite experiencing heavy anthropogenic aerosol dimming at the surface, a region need not necessarily show strong SST changes, for example, because of interference with heat transport by ocean currents or because of aerosol-induced changes in ocean currents. Moreover, SSR reductions need not necessarily lead to SST changes but can be compensated by other surface energy fluxes, e.g., long-wave radiation. Therefore, further research will focus on such aspects using modeling frameworks with interactive oceans, bearing in mind the results presented here.

Appendix A

A1. Identify Anthropogenically Forced Grid Cells

From the data in CTRL we generate a reference distribution of the three variables, AOD, clearlsky SSR, and all-sky SSR for each grid cell. These variables potentially reflect anthropogenic aerosol dimming in a relatively direct manner. Because of the clear seasonality of anthropogenic aerosol dimming in Figure 5, a reference distribution is generated for each month. Given that the reference distribution is generated from data from nine CTRL ensemble members over 130 years, the reference distribution can be viewed as a sufficiently robust anchor (sample size 1170 for each grid point and month) for further data analysis.

We compare ANTH ensemble data at each grid point with the CTRL reference distribution. Because we are interested in the temporal evolution of the plumes, their shape, area, and average properties as a function of time, we split the ANTH data into decadal chunks. Since we have 13 ensemble members in ANTH, this adds up to a sample size of 130 for each decade and month at each grid point.

The data do not fit a parametric distribution. Therefore, we use nonparametric approaches to identify whether a grid cell can be classified as being anthropogenically influenced. For each variable we define a statistical threshold indicative of anthropogenic aerosol effects to be applied at each grid point for each month. The respective criteria are outlined in the sections to follow. The principle is to count how often the values in the ANTH sample exceed the threshold. An illustration of how frequently the 50th percentile as a statistical threshold is triggered is shown in Figure 6. The 90th quantile exceedance fraction for AOD (10th quantile for SSR) is shown in Figure 7. To go from this exceedance fraction to anthropogenically influenced plumes, we somewhat arbitrarily define a grid cell as anthropogenically influenced if more than 50% of the 130 samples exceed the threshold within a grid cell. The 90th or 10th percentile depending on variable analyzed together with the 50% exceedance fraction criterion for plume selection provides a very strict criterion so that we focus on grid points which are not only strongly but also often affected by anthropogenic aerosols.

A2. Identify Coherent Plume Structures

As evident in Figure 5, the aerosol dimming shows plume-like characteristics. Therefore, we do not select all grid points that yield a positive result to our test but only select coherent areas which turn out to be attached to continents from where anthropogenic aerosols are predominantly emitted and transported out to sea. The only exceptions are ship and airplane emissions, which are negligible compared to the continental emissions. To determine coherent areas, for each plume region, we select a longitude-latitude area, which covers the entire extent of a plume as seen in Figure 5. Within this area, we remove outlying positive grid points by applying a noise removal filter, as it is used in image processing. The pixel-wise adaptive Wiener filter [*Lim*, 1990] uses the mean (μ) and variance (σ^2) of the values around each pixel—or in our case grid cell—to perform the smoothing as shown in equation (A1). The variables $a(n_1, n_2)$ and $b(n_1, n_2)$ represent the intensity of the entity considered before and after the smoothing process, respectively. The variables n_1 and n_2 determine how many neighboring grid cells are chosen around each grid cell (a). In our case these values were both set to three grid cells so that a square of 3×3 grid cells was used to derive μ and σ^2. The ν is the noise variance, which is defined as the average of all local variances in the vicinity of the grid cell in question. The noise is defined as Gaussian white noise.

$$b(n_1, n_2) = \mu + \frac{\sigma^2 - \nu^2}{\sigma^2}(a(n_1, n_2) - \mu^2) \tag{A1}$$

After this step, the size and intensity of the plume regions identified can be derived as well as the inter-decadal evolution of each plume. The results of the analyses are shown in sections 3.2 and 3.3.

In the following sections, we will touch upon the particularities of each of the variables considered. The shapes of the respective PDFs are shown in Figure A1. The data shown stem from a single grid box in the Indian Ocean (7°N, 81°E), which is affected by anthropogenic aerosol dimming. For illustrative purposes, the data sets shown in Figure A1 have been smoothed using a kernel function. This step was not employed in the actual analysis.

A3. AOD

AOD is an easier variable to interpret than SSR. Its magnitude is not affected by the Earth's inclination and orbit around the Sun (variations in insolation from pole to equator and seasonal cycles), nor does it show impacts from major volcanic eruptions. The latter are prescribed in the form of stratospheric optical thickness bands (see section 2.1). The PDF of AOD (Figure A1, top) is bounded at zero AOD and is positively skewed with a maximum around 0.1. Negative values seen in Figure A1 are an artifact from smoothing. From this Figure, it is evident that anthropogenic aerosols mainly affect the right tail of the distribution. Therefore, a simple test to check a grid box for anthropogenic AOD is to quantify how often the 90th percentile of the CTRL distribution is exceeded. Exceedance frequencies higher than 50% indicate a commonly occurring and—considering the CTRL data set—extreme AOD in ANTH.

A4. Clear-Sky SSR

Identifying aerosol plumes based on downward clear-sky SSR is a more direct approach since clear-sky SSR is a component of the surface energy balance, which determines SSTs. However, clear-sky SSR is also more complex since it varies with latitude and time due to the Earth's inclination and orbit around the Sun. Moreover, the variable includes the impact of major volcanic eruptions, which can sometimes be more pronounced than anthropogenic dimming.

In the approach chosen, latitudinal and seasonal variations in SSR are largely removed by comparing the two ensembles, CTRL and ANTH, on a grid cell by grid cell and month-to-month basis for each decade. The effect of volcanic eruptions is removed by subtracting the ensemble mean of the CTRL ensemble (monthly time steps) from each individual member of both the CTRL and ANTH ensembles before proceeding with the actual analysis. As evident in Figure A1 (middle), the anthropogenic aerosol signal in clear-sky SSR leads to a slight increase in spread and a general shift of the distribution to the left.

Unlike AOD, the reference PDF of clear-sky SSR has tails on either side of the distribution but is not always normally distributed. As we are interested in dimming, i.e., in a reduction of SSR due to anthropogenic aerosols, we define the criterion such that grid cells with less incoming solar radiation compared to the CTRL ensemble are identified. The threshold value is the 10th quantile of each reference distribution. A grid box is classified as of anthropogenic influence if 50% of the 130 ANTH samples fall below the 10% quantile of the reference distribution.

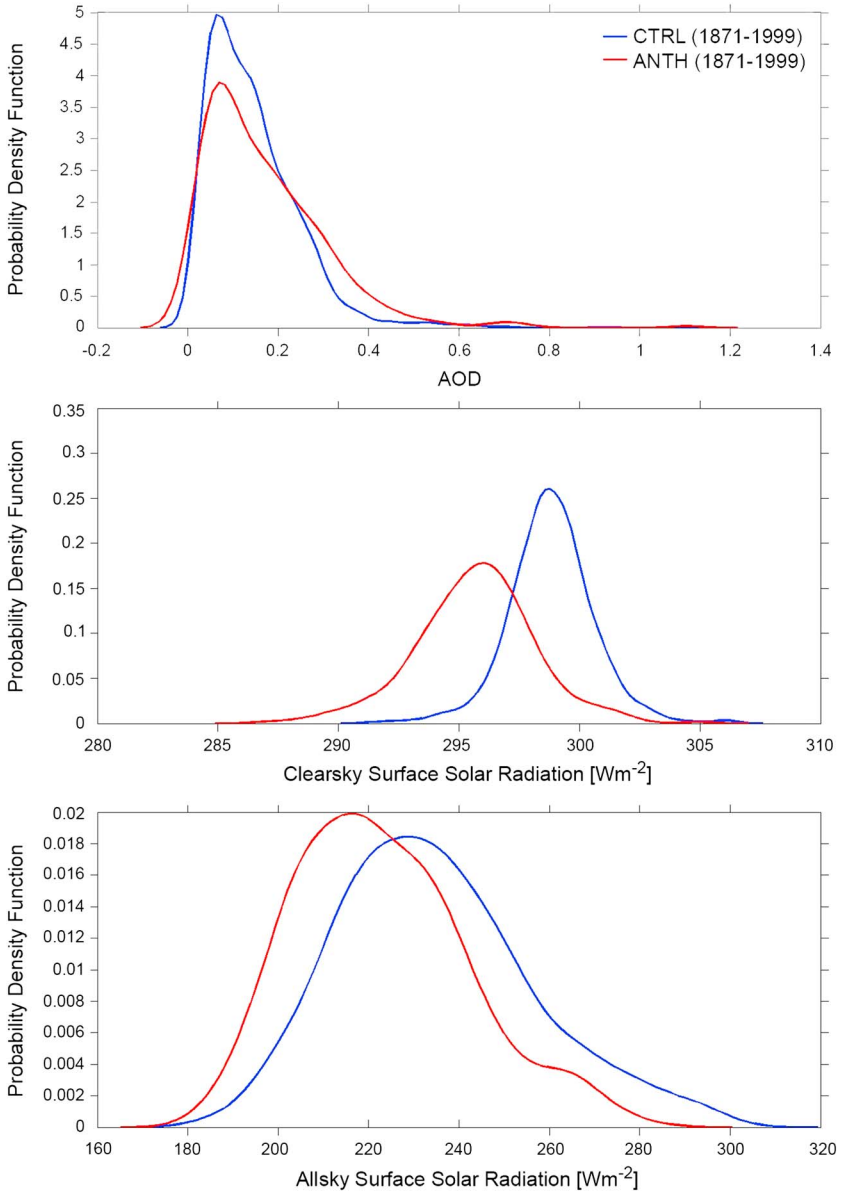

Figure A1. Examples of probability density functions from the CTRL (blue) and ANTH (red) data sets for (top) AOD, (middle) clear-sky SSR, and (bottom) all-sky SSR. Data stem from one grid box (7°N, 81°E) and cover the years 1871–1999 for both CTRL and ANTH. For illustrative purposes, a kernel smoothing function was applied to the data sets, which was not used for the actual data analysis.

A5. All-Sky SSR

All-sky SSR differs from clear-sky SSR in that it also accounts for cloud radiative effects. Hence, in a sense, it may also be viewed as a rough approximation of the indirect aerosol effect. However, it is not only aerosol effects that determine changes in cloud cover but also circulation changes or changes in atmospheric stability, which makes the variable noisier and more difficult to interpret. In Figure A1 (bottom) it is shown that the reference PDF (CTRL) has a considerable spread due to natural cloud variability. Anthropogenic aerosols mainly cause a change in the mean of the distribution but hardly affect the width of the data set. Nevertheless, similar to clear-sky SSR, a decrease in density at the right-hand tail density is seen, while the left-hand tail of the distribution experiences an increase in density. However, the lower end of the distribution does not show an equally pronounced tail as seen for clear-sky SSR. We apply the same criterion for anthropogenic aerosol influence as for clear-sky SSR, i.e., exceeding the 10th quantile for at least half of all the data in the distribution.

Acknowledgments
This work is supported by ETH research grant CH2-0111-1. We acknowledge the support by the ETH Foundation as well as the Centre for Climate Systems Modelling, C2SM. Computations were performed at the Swiss National Supercomputing Center, CSCS, Manno. The authors thank the MPI Hamburg for providing access to the ECHAM5-HAM code and colleagues at ETH Zürich who contributed to model development. Model output data used for this work are stored at ETH Zürich and can be requested via email (tanja.dallafior@env.ethz.ch). Remote observational data analyses used in Figure 2 were produced with the Giovanni online data system, developed and maintained by the NASA GES DISC.

References

Albrecht, B. (1989), Aerosols, cloud microphysics, and fractional cloudiness, *Science*, *245*(4923), 1227–1230.
Bichet, A., M. Wild, and C. Schär (2011), Global precipitation response to changing forcings since 1870, *Atmos. Chem. Phys.*, *11*, 9961–9970.
Bollasina, M., Y. Ming, and V. Ramaswamy (2011), Anthropogenic aerosols and the weakening of the south Asian Summer Monsoon, *Science*, *334*(6055), 502–505.
Booth, B., N. Dunstone, P. Halloran, T. Andrews, and N. Bellouin (2012), Aerosols implicated as a prime driver of twentieth-century North Atlantic climate variability, *Nature*, *484*(7393), 228–232.
Chang, C.-Y., J. Chiang, M. Wehner, A. Friedman, and R. Ruedy (2011), Sulfate aerosol control of tropical Atlantic climate over the twentieth century, *J. Clim.*, *24*(10), 2540–2555.
Chiang, J. C. H., C.-Y. Chang, and M. Wehner (2013), Long-term behavior of the Atlantic interhemispheric SST gradient in the CMIP5 historical simulations, *J. Clim.*, *26*(21), 8628–8640.
Chung, C., and V. Ramanathan (2006), Weakening of North Indian SST gradients and the monsoon rainfall in India and the Sahel, *J. Clim.*, *19*(10), 2036–2045.
Cowan, T., and W. Cai (2013), The response of the large-scale ocean circulation to 20th century Asian and non-Asian aerosols, *Geophys. Res. Lett.*, *40*, 2761–2767, doi:10.1002/grl.50587.
Cox, P., P. Harris, C. Huntingford, R. Betts, M. Collins, C. Jones, T. Jupp, J. Marengo, and C. Nobre (2008), Increasing risk of Amazonian drought due to decreasing aerosol pollution, *Nature*, *453*(7192), 212–216.
Delworth, T., V. Ramaswamy, and G. L. Stenchikov (2005), The impact of aerosols on simulated ocean temperature and heat content in the 20th century, *Geophys. Res. Lett.*, *32*, L24709, doi:10.1029/2005GL024457.
Dunstone, N., B. Booth, L. Hermanson, and R. Eade (2013), Anthropogenic aerosol forcing of Atlantic tropical storms, *Nat. Geosci.*, *6*(7), 534–539.
Evan, A., D. Vimont, A. Heidinger, J. Kossin, and R. Bennartz (2009), The role of aerosols in the evolution of tropical north Atlantic ocean temperature anomalies, *Science*, *324*(5928), 778–781.
Folini, D., and M. Wild (2011), Aerosol emissions and dimming/brightening in Europe: Sensitivity studies with ECHAM5-HAM, *J. Geophys. Res.*, *114*, D21104, doi:10.1029/2011JD016227.
Fouquart, Y., and B. Bonnel (1980), Computations of solar heating of the Earth's atmosphere—A new parameterization, *Beiträge zur Phys. der Atmos.*, *53*, 35–62.
Hansen, J., M. Sato, A. Lacis, R. Ruedy, I. Tegen, and E. Matthews (1998), Climate forcings in the industrial era, *Proc. Natl. Acad. Sci.*, *95*, 12,753–12,758.
Haywood, J., N. Bellouin, A. Jones, O. Boucher, M. Wild, and K. Shine (2011), The roles of aerosol, water vapor and cloud in future global dimming/brightening, *J. Geophys. Res.*, *116*, D20203, doi:10.1029/2011JD016000.
Hsieh, W.-C., W. Collins, Y. Liu, J. Chiang, C.-Y. Shie, K. Caldeira, and L. Cao (2013), Climate response due to carbonaceous aerosols and aerosol-induced SST effects in NCAR community atmospheric model CAM3.5, *Atmos. Chem. Phys.*, *13*(15), 7489–7510.
Intergovernmental Panel on Climate Change (IPCC) (2013), *Climate Change 2013: The Physical Science Basis. Contribution of Working Group I to the Fifth Assessment report of the Intergovernmental Panel on Climate Change*, 1535 pp., Cambridge Univ. Press, Cambridge, U. K., and New York.
Johnson, B., K. Shine, and P. Forster (2004), The semi-direct aerosol effect: Impact of absorbing aerosols on marine stratocumulus, *Q. J. R. Meteorol. Soc.*, *130*, 1407–1422.
Jones, A., J. Haywood, and O. Boucher (2007), Aerosol forcing, climate response and climate sensitivity in the Hadley Centre climate model, *J. Geophys. Res.*, *112*, D20211, doi:10.1029/2007JD008688.
Kaufman, Y., D. Tanré, and O. Boucher (2002), A satellite view of aerosols in the climate system, *Nature*, *419*, 215–223.
Kettle, A., and M. Andreae (2000), Flux or dimethylsulfide from the oceans: A comparison of updated data sets and flux models, *J. Geophys. Res.*, *105*(D22), 26,793–26,808.
Kiehl, J., T. Schneider, R. Portmann, and S. Solomon (1999), Climate forcing due to tropospheric and stratospheric ozone, *J. Geophys. Res.*, *104*(D14), 31,239–31,254.
Koch, D., S. Menon, A. D. Genio, R. Ruedy, I. Alienov, and G. Schmidt (2009), Distinguishing aerosol impact on climate over the past century, *J. Clim.*, *22*, 2659–2677.
Lim, J. (1990), *Two-Dimensional Signal and Image Processing*, 548 pp., Prentice Hall, Upper Saddle River, N. J.
Lin, S., and R. Rood (1996), An explicit flux-form semi-Lagrangian shallow-water model on the sphere, *Mon. Weather Rev.*, *122*, 2046–2070.
Lohmann, U., and J. Feichter (2005), Global indirect aerosol effects: A review, *Atmos. Chem. Phys.*, *5*, 715–737.
Lohmann, U., and E. Roeckner (1996), Design and performance of a new cloud microphysics schmee developed for the ECHAM general circulation model, *Clim. Dyn.*, *12*, 557–572.
Lohmann, U., P. Stier, C. Hoose, S. Ferrachat, S. Kloster, E. Roeckner, and J. Zhang (2007), Cloud microphysics and aerosol indirect effects in the global climate model ECHAM5-HAM, *Atmos. Chem. Phys.*, *7*, 3425–3446.
Lohmann, U., L. Rotstayn, T. Storelvmo, A. Jones, S. Menon, J. Quaas, A. Ekman, D. Koch, and R. Ruedy (2010), Total aerosol effect: Radiative forcing or radiative flux perturbation?, *Atmos. Chem. Phys.*, *10*, 3235–3246.
Martin, E., C. Thorncroft, and B. Booth (2014), The multidecadal Atlantic SST-sahel rainfall teleconnection in CMIP5 simulations, *J. Clim.*, *27*, 784–806.
Ming, Y., and V. Ramaswamy (2011), A model investigation of aerosol-induced changes in tropical circulation, *J. Clim.*, *24*, 5125–5133.
Mlawer, E., S. Taubman, P. Brown, M. Iacono, and S. Clough (1997), Radiative transfer for inhomogeneous atmospheres: RRTM, a validated correlated-k model for the longwave, *J. Geophys. Res.*, *102*(D14), 16,663–16,682.
Monahan, E., D. Spiel, and K. Davidson (1986), A model of marine aerosol generation via whitecaps and wave disruption, in *Oceanic Whitecaps and Their Role in Air-Sea Exchange Processes*, edited by E. Monahan, G. MacNiocaill and D. Reidel, pp. 167–174, Dordrecht, Netherlands.
Morcrette, J.-J., S. Clough, E. Mlawer, and M. Iacono (1998), Impact of a validated radiative transfer scheme, RRTM, on the ECMWF model climate and 10-day forecasts, *Tech. Memo.*, *252*, 47.
Myhre, G., et al. (2005), Intercomparison of satellite retrieved aerosol optical depth over ocean during the period September 1997 to December 2000, *Atmos. Chem. Phys.*, *5*, 1697–1719.
Nightingale, P., G. Malin, C. Law, A. Watson, P. Liss, M. Liddicoat, J. Boutin, and R. Upstill-Goddard (2000), In situ evaluation of air-sea gas exchange parameterizations using novel conservative and volatile tracers, *Global Biogeochem. Cycles*, *14*, 373–387.
Nordeng, T. (1994), *Extended Versions of the Convective Parametrization Scheme at ECMWF and Their Impact on the Mean and Transient Activity of the Model in the Tropics*, European Centre for Medium-Range Weather Forecasts, Reading, England.

Nozawa, T., T. Nagashima, T. Ogura, T. Yokohata, and N. Okada (2007), Climate change simulations with a coupled ocean-atmosphere GCM called the model for interdisciplinary research on climate. [Available at http://www.cger.nies.go.jp/publications/report/i073/I073.pdf.]

Persad, G., Y. Ming, and V. Ramaswamy (2014), The role of aerosol absorption in driving clear-sky solar dimming over east Asia, *J. Geophys. Res. Atmos.*, *119*, 10,410–10,424, doi:10.1002/2014JD021577.

Ramanathan, V., and G. Carmichael (2008), Global and regional climate changes due to black carbon, *Nat. Geosci.*, *109*, 221–227.

Ramanathan, V., and Y. Feng (2009), Air pollution, greenhouse gases and climate change: Global and regional perspectives, *Atmos. Environ.*, *43*, 37–50.

Ramanathan, V., et al. (2001), Indian Ocean Experiment: An integrated analysis of the climate forcing and effects of the great Indo-Asian haze, *J. Geophys. Res.*, *106*(D22), 28,371–28,398.

Ramanathan, V., C. Chung, D. Kim, T. Bettge, L. Buja, J. Kiehl, W. Washington, Q. Fu, D. Sikka, and M. Wild (2005), Atmospheric brown clouds: Impacts on South Asian climate and hydrological cycle, *Proc. Natl. Acad. Sci.*, *102*(15), 5326–5333.

Ramaswamy, V., et al. (2001), Radiative forcing of climate change, in *Climate Change 2001: The Scientific Basis. Contribution of Working Group I to the Third Assessment Report of the Intergovernmental Panel on Climate Change*, edited by J. T. Houghton et al., pp. 349–416, Cambridge Univ. Press, Cambridge, U. K., and New York.

Rayner, N., D. Parker, E. Horton, C. Folland, L. Alexander, D. Rowell, E. Kent, and A. Kaplan (2003), Global analyses of sea surface temperature, sea ice, and night marine air temperature since the late nineteenth century, *J. Geophys. Res.*, *108*(D14), 4407, doi:10.1029/2002JD002670.

Roeckner, E., et al. (2003), The atmospheric general circulation model ECHAM5: Part 1: Model description, *Rep. 239*, Max Planck Institute for Meteorology, Hamburg, Germany.

Roeckner, E., P. Stier, J. Feichter, S. Kloster, M. Esch, and I. Fischer-Bruns (2006), Impact of carbonaceous aerosol emissions on regional climate change, *Clim. Dyn.*, *27*, 553–571.

Roelofs, G.-J. (2012), Aerosol lifetime and climate change, *Atmos. Chem. Phys.*, *12*, 116,493–16,514.

Romanou, A., B. Liepert, G. Schmidt, W. Rossow, R. Ruedy, and Y. Zhang (2007), 20th century changes in surface solar irradiance in simulations and observations, *Geophys. Res. Lett.*, *34*, L05713, doi:10.1029/2006GL028356.

Rotstayn, L., and U. Lohmann (2002), Tropical rainfall trends and the indirect aerosol effect, *J. Clim.*, *15*, 2103–2116.

Sato, M., J. Hansen, M. McCormick, and J. Pollack (1993), Stratospheric aerosol optical depths, 1850-1990, *J. Geophys. Res.*, *98*, 22,987–22,994.

Schutgens, N., M. Nakata, and T. Nakajima (2013), Validation and empirical correction of MODIS AOT and AE over ocean, *Atmos. Meas. Tech.*, *6*, 2355–2475.

Shindell, D. T., A. Voulgarakis, F. Faluvegi, and G. Milly (2012), Precipitation response to regional radiative forcing, *Atmos. Chem. Phys.*, *12*, 6969–6982.

Solanki, S., and N. Krivova (2003), Can solar variability explain global warming since 1970?, *J. Geophys. Res.*, *108*(A5), 1200, doi:10.1029/2002JA009753.

Stier, P., et al. (2005), The aerosol-climate model ECHAM5-HAM, *Atmos. Chem. Phys.*, *5*, 1125–1156.

Stier, P., J. Feichter, E. Roeckner, S. Kloster, and M. Esch (2006a), The evolution of the global aerosol system in a transient climate simulation from 1860 to 2100, *Atmos. Chem. Phys.*, *6*, 3059–3076.

Stier, P., J. Feichter, S. Kloster, E. Vignati, and J. Wilson (2006b), Emission-induced nonlinearities in the global aerosol system: Results from the ECHAM5-HAM aerosol-climate model, *J. Clim.*, *19*, 3845–3862.

Stier, P., et al. (2013), Host model uncertainties in aerosol radiative forcing estimates: Results from the AeroCom prescribed intercomparison study, *Atmos. Chem. Phys.*, *13*, 3245–3270.

Sundqvist, H., E. Berge, and J. Kristjansson (1989), Condensation and cloud parameterization studies with a mesoscale numerical weather prediction model, *Mon. Weather Rev.*, *8*, 1641–1657.

Tegen, I., S. Harrison, K. Kohfeld, I. Prentice, M. Coe, and M. Heimann (2002), Impact of vegetation and preferential source areas on global dust aerosol: Results from a model study, *J. Geophys. Res.*, *107*(D21), 1984–2012.

Textor, C., et al. (2007), The effect of harmonized emissions on aerosol properties in global models—An AeroCom experiment, *Atmos. Chem. Phys.*, *7*, 4489–4501.

Tiedtke, M. (1989), A comprehensive mass flux scheme for cumulus parameterization in large-scale models, *Mon. Weather Rev.*, *117*(8), 1779–1800.

Trenberth, K., et al. (2007), Observations: Surface and atmospheric climate change, in *Climate Change 2007: The Physical Science Basis. Contribution of Working Group I to the Fourth Assessment Report of the Intergovernmental Panel on Climate Change*, edited by S. Solomon et al., Cambridge Univ. Press, Cambridge, U. K., and New York.

Twomey, S. (1977), The influence of Pollution on the Shortwave Albedo of Clouds, *J. Atmos. Sci.*, *34*(7), 1149–1154.

Vignati, E., and J. Wilson (2004), M7: An efficient size-resolved aerosol microphysics module for large-scale aerosol transport models, *J. Geophys. Res.*, *109*, D22202, doi:10.1029/2003JD004485.

Wild, M. (2009), Global dimming and brightening: A review, *J. Geophys. Res.*, *114*, D00D16, doi:10.1029/2008JD011470.

Wild, M. (2012), Enlightening global dimming and brightening, *Bull. Am. Meteorol. Soc.*, *93*, 27–37.

Wild, M., and B. Liepert (2010), The Earth radiation balance as driver of the global hydrological cycle, *Environ. Res. Lett.*, *5*, 025003.

Yu, H., et al. (2006), A review of measurement-based assessments of the aerosol direct radiative effect and forcing, *Atmos. Chem. Phys.*, *6*, 613–666.

Zhang, R., et al. (2013), Have aerosols caused the observed Atlantic multidecadal variability?, *J. Atmos. Sci.*, *70*, 1135–1144.